



# Dynamic wave–soil–structure interaction analysis in the time domain

J.L. Wegner<sup>a,\*</sup>, M.M. Yao<sup>a</sup>, X. Zhang<sup>b</sup>

<sup>a</sup> *Department of Mechanical Engineering, University of Victoria, P.O. Box 3055, Victoria, BC, Canada V8W 3P6*

<sup>b</sup> *Department of Engineering Mechanics, Tsinghua University, Beijing 100084, People's Republic of China*

Received 20 July 2004; accepted 25 April 2005

Available online 20 July 2005

## Abstract

In recent papers [Zhang X, Wegner JL, Haddow, JB. Three dimensional soil–structure–wave interaction analysis in time domain. *Earthq Eng Struct Dynam* 1999;36:1501–24; Wegner, JL, Zhang X. Free vibration analysis of a three-dimensional soil–structure system. *Earthq Eng Struct Dynam* 2001;30:43–57], a new numerical procedure was developed and implemented into a three-dimensional dynamic soil–structure interaction analysis program (DSSIA-3D). In this novel procedure, a substructure method is used in which the unbounded soil is modeled by the scaled boundary finite-element method and the structure is modeled by a standard FEM. This results in an improvement over current methods. In this paper, we apply DSSIA-3D to obtain the dynamic response of tall buildings, with multi-level basements, subjected to realistic seismic excitations, including P-, SV-, and SH-waves, at various angles of incidence. Numerical results are obtained for the dynamic response of the soil–structure system, which depends upon frequency content, wave pattern and input angle of ground motion.

© 2005 Elsevier Ltd. All rights reserved.

*Keywords:* Wave–soil–structure interaction; Substructure method; Scaled boundary finite-element method

## 1. Introduction

In a recent paper by Zhang et al. [1], a new numerical procedure (DSSIA-3D) was formulated for the analysis of three-dimensional dynamic soil–structure in the time domain. DSSIA-3D can be used in the analyses of three-dimensional dynamic soil–structure interaction as well as in the analysis of wave scattering and diffraction by three-dimensional surface irregularities. In that study, the scattering and diffraction of seismic waves

by various three-dimensional surface irregularities were studied in detail, and the numerical results obtained were in good agreement with those given by others. In a later paper by Wegner and Zhang [2], DSSIA-3D was applied to obtain the dynamic response of a spherical cavity, embedded in full-space, subjected to seismic waves. In that study, the numerical results were compared to the analytical solutions, with excellent agreement. Also in that study, DSSIA-3D was then successfully applied to obtain the three-dimensional, free vibration of a dam–foundation system. The objective of the present study is to apply DSSIA-3D to obtain the dynamic response of tall buildings, with multi-level basements, subjected to realistic seismic excitations, including P-, SH-, SV-waves, at various angles of incidence.

\* Corresponding author. Tel.: +1 250 721 8694; fax: +1 250 721 6051.

E-mail address: [jwegner@uvic.ca](mailto:jwegner@uvic.ca) (J.L. Wegner).

Numerical results are obtained for the dynamic response of the soil–structure system, which depends upon frequency content, wave pattern, and input angle of ground motion.

The dynamic soil–structure interaction (SSI) attracts great interest in the civil engineering, the nuclear power industry, and underground communication facilities designers communities. There are a few methods, which can be adopted to approximate and simulate the SSI system and different solutions have been achieved with different levels of accuracy. In recent years, several novel numerical methods have been developed, including the scaled boundary finite-element method [3] and some hybrid methods [4,5]. All of these methods can be classified into two main categories: the direct method and the substructure method.

In the direct method, the structure and a finite, bounded soil zone adjacent to the structure (near field) are modeled by the standard finite-element method and the effect of the surrounding unbounded soil (far field) is analyzed approximately by imposing transmitting boundaries along the near-field/far-field interface. Many kinds of transmitting boundaries have been developed over the past two decades to satisfy the radiation condition, such as a viscous boundary [6], a superposition boundary [7], and several others [8].

The substructure method is more complex than the direct method in modeling the SSI system. In the substructure method, the soil–structure system is divided into two substructures: a structure, which may include a portion of non-linear soil or soil with an irregular boundary, and the unbounded soil [3,9]. These substructures are connected by the general soil–structure interface, as shown in Fig. 1. In this study, the unbounded soil is assumed to be a linear elastic solid, but the unbounded soil could be non-linear in further studies.

Usually a dynamic soil–structure interaction analysis by the substructure method can be performed in three steps as follows:

1. Determination of seismic free-field input motion along the general soil–structure interface.

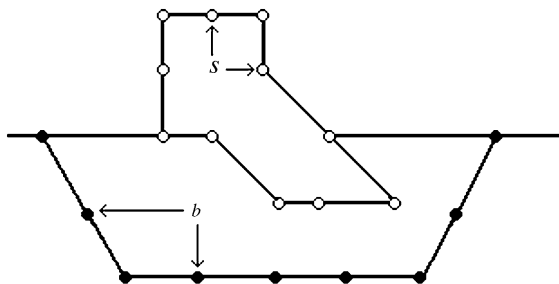


Fig. 1. A soil–structure interaction system.

2. Determination of the reaction of the unbounded soil on the general soil–structure interface in the form of a displacement–force relationship.
3. Analysis of the bounded soil–structure system under the action of the externally applied transient loading and the ground interaction force determined by steps 1 and 2.

The reaction of the unbounded soil on the general soil–structure interface is represented by a boundary condition in the form of force–displacement relationship, which is global in both space and time. The boundary-element method is a powerful procedure for modeling the unbounded medium since only the boundaries of the unbounded medium are discretized so that the spatial dimension is reduced by 1, and the radiation condition is satisfied automatically as a part of the fundamental solution. Based on the substructure method, many hybrid methods (coupling methods) [6–8] have been developed where the structure and an adjacent finite region of the soil are discretized by the standard finite-element method while the unbounded soil is modeled by the boundary-element method. However, it is very difficult to derive the fundamental solutions for many cases. The scaled boundary finite-element method [10], which is the alias of the consistent infinitesimal finite-element cell method [11], combines the advantages of the boundary-element method and the finite-element method, and no fundamental solution is required. It is exact in the radial direction, converges to the exact solution in the finite-element sense in the circumferential direction, and is rigorous in both space and time.

The novel three-dimensional dynamic soil–structure interaction procedure (DSSIA-3D) [1,2] uses the scaled boundary finite-element method to model the unbounded soil while the structure is modeled using standard finite-element method. In this numerical procedure, approximations in both time and space, which lead to efficient schemes for calculation of the acceleration unit-impulse response matrix, are implemented in the scaled finite-element method resulting in an order of magnitude reduction in the required computational effort when compared to other methods. Mathematical details of DSSIA-3D can be found in [1].

In this paper, DSSIA-3D is applied to obtain the dynamic response of various tall buildings, with multi-level basements, which are subjected to seismic waves. The response of tall buildings' vibration during a large seismic motion is of great interest to the research community. Recent literature on this subject contains numerical results using the direct method [12]. Because the direct method is employed, results obtained in that study neglect the effect of the adjacent soil on the amplitude of the structure's motion and damping ratio of the soil, which is an important factor. Also, in order to achieve

the proper accuracy and reduce the effects of reflected waves by the transmitting boundary, it is necessary to consider a large amount of soil around the structure when the direct method is employed. Consequently, the application of DSSIA-3D is extremely advantageous to this problem because this numerical procedure can account for the soil structure interaction effects, and also the computational effort is significantly reduced. In this paper, P-, SH-, and SV-waves are considered as input waves based on the Tabas earthquake recording (Iran, 1978), which was also used in the study by Tehranizadeh [12].

## 2. Governing equations

If both seismic excitation and externally applied transient loading are considered, the equation of motion of the structure in the time domain can be expressed as [2]

$$\begin{aligned} & \begin{bmatrix} \mathbf{M}_{ss} & \mathbf{M}_{sb} \\ \mathbf{M}_{bs} & \mathbf{M}_{bb} \end{bmatrix} \begin{Bmatrix} \ddot{\mathbf{u}}_s^t \\ \ddot{\mathbf{u}}_b^t \end{Bmatrix} + \begin{bmatrix} \mathbf{C}_{ss} & \mathbf{C}_{sb} \\ \mathbf{C}_{bs} & \mathbf{C}_{bb} \end{bmatrix} \begin{Bmatrix} \dot{\mathbf{u}}_s^t \\ \dot{\mathbf{u}}_b^t \end{Bmatrix} \\ & + \begin{bmatrix} \mathbf{K}_{ss} & \mathbf{K}_{sb} \\ \mathbf{K}_{bs} & \mathbf{K}_{bb} \end{bmatrix} \begin{Bmatrix} \mathbf{u}_s^t \\ \mathbf{u}_b^t \end{Bmatrix} \\ & = \begin{Bmatrix} 0 \\ -\mathbf{r}_b(t) \end{Bmatrix} + \begin{Bmatrix} \mathbf{p}_s(t) \\ \mathbf{p}_b(t) \end{Bmatrix}, \end{aligned} \quad (1)$$

where  $\mathbf{M}$  is the mass matrix,  $\mathbf{K}$  is the stiffness matrix of the structure,  $\mathbf{u}$ ,  $\dot{\mathbf{u}}$ , and  $\ddot{\mathbf{u}}$  are the displacement, velocity, and acceleration vectors, respectively,  $\mathbf{r}_b(t)$  is the ground interaction force vector, and  $\mathbf{p}(t)$  are externally applied force vectors. In Eq. (1), the subscripts  $b$  and  $s$  denote the nodes on the soil–structure interface and the nodes of the building, respectively, as shown in Fig. 1. The superscript  $t$  represents the total motion of the structure. The damping matrix  $\mathbf{C}$  represents viscous damping in the structure and is included for completeness but is not considered in the numerical examples presented later in this paper.

In this study, we consider structures subjected to seismic waves only, consequently the external forces on the structure,  $\mathbf{p}(t)$ , are set equal to zero. After the ground interaction force vector,  $\mathbf{r}_b(t)$ , is determined, the dynamic response of the structure can be obtained from Eq. (1) by using direct integration. Details of the numerical integration methods employed can be found in [1].

## 3. Ground interaction force

In the substructure method, the ground interaction forces  $\mathbf{r}_b(t)$  are given by the convolution integral [1],

$$\mathbf{r}_b(t) = \int_0^t \mathbf{M}_{bb}^g(t-\tau)(\dot{\mathbf{u}}_b^g(\tau) - \ddot{\mathbf{u}}_b^g(\tau)) d\tau, \quad (2)$$

where the superscript  $g$  represents the unbounded ground soil with excavation,  $\mathbf{M}_{bb}^g(t)$  is the acceleration unit-impulse matrix, and  $\ddot{\mathbf{u}}_b^g(t)$  is the acceleration vector, at the nodes  $b$  (which will subsequently lie on the structure–soil interface) of the soil with the excavation. Eq. (2) can be used to calculate a general wave pattern consisting of oblique body waves and surface waves. The ground motion  $\ddot{\mathbf{u}}_b^g(t)$  depends on the excavation so that it is more convenient to replace this generalized scattered motion by the free-field motion  $\ddot{\mathbf{u}}_b^f(t)$ , which does not depend on the excavation, with the exception of the location of the nodes for which it is to be calculated, and can be determined by the free-field site analysis [3,13].

The free-field system results when the excavated part of the soil is added to the soil with excavation as indicated in Fig. 1. For this special case, the structure consists of the excavated part of the soil only, and part of the integral on the right-hand side of Eq. (2) can be reformulated by considering the equation of motion as [1]

$$\int_0^t \mathbf{M}_{bb}^g(t-\tau)\ddot{\mathbf{u}}_b^g(\tau) d\tau = \int_0^t \mathbf{M}_{bb}^f(t-\tau)\ddot{\mathbf{u}}_b^f(\tau) d\tau, \quad (3)$$

where  $\mathbf{M}_{bb}^f$  is the acceleration unit-impulse response matrix of the free-field site referred to the nodes at the soil–structure interface. To calculate the acceleration unit-impulse response matrix of the free field site, the excavated part of the soil is discretized by the finite-element method. Standard finite-element discretization of the excavated part of the soil results in the acceleration unit-impulse response matrix  $\mathbf{M}^e$  of the excavated soil, which is given by

$$\mathbf{M}^e = -\frac{1+2\zeta i}{\omega^2} \mathbf{K}_e + \mathbf{M}_e, \quad (4)$$

where  $\mathbf{K}_e$  is the stiffness matrix of the excavated soil,  $\mathbf{M}_e$  is the mass matrix,  $\omega$  is the circular frequency,  $i = \sqrt{-1}$ , and  $\zeta$  is the hysteretic damping ratio of the excavated soil. The matrix  $\mathbf{M}^e$  can be decomposed into the submatrices  $\mathbf{M}_{ii}$ ,  $\mathbf{M}_{ib}$  and  $\mathbf{M}_{bb}$ . The subscript  $b$  refers to the nodes on the structure–soil interface, and the subscript  $i$  refers to the remaining nodes. Eliminating the degree of freedom at the  $i$ th node leads to

$$\mathbf{M}_{bb}^e = \mathbf{M}_{bb} - \mathbf{M}_{bi}\mathbf{M}_{ii}^{-1}\mathbf{M}_{ib}, \quad (5)$$

where  $\mathbf{M}_{bb}^e$  denotes the acceleration unit-impulse response matrix of the excavated soil referred to the nodes  $b$ . Adding  $\mathbf{M}_{bb}^e$  to  $\mathbf{M}_{bb}^g$  results in the acceleration unit-impulse response matrix of the continuous soil (free-field site, refer to Fig. 1)  $\mathbf{M}_{bb}^f$ , discretized at the same nodes  $b$ , which subsequently lie on the structure–soil interface. That is,

$$\mathbf{M}_{bb}^f = \mathbf{M}_{bb}^e + \mathbf{M}_{bb}^g. \quad (6)$$

Substituting Eqs. (6) and (3) into Eq. (2) gives

$$\mathbf{r}_b(t) = \mathbf{r}_b^{(1)}(t) + \mathbf{r}_b^{(2)}(t), \quad (7)$$

where

$$\mathbf{r}_b^{(1)}(t) = \int_0^t \mathbf{M}_{bb}^g(t-\tau)(\ddot{\mathbf{u}}_b^t(\tau) - \ddot{\mathbf{u}}_b^f(\tau)) d\tau,$$

$$\mathbf{r}_b^{(2)}(t) = - \int_0^t \mathbf{M}_{bb}^e(t-\tau)\ddot{\mathbf{u}}_b^f(\tau) d\tau.$$

The acceleration unit-impulse response matrix  $\mathbf{M}_{bb}^g(t)$  is calculated using the scaled boundary finite-element method [3]. It may be shown that

$$\mathbf{r}_b^{(2)}(t) = -F^{-1}[\mathbf{M}_{bb}^e(\omega)\ddot{\mathbf{u}}_b^f(\omega)], \quad (8)$$

where  $F^{-1}[*]$  denotes the Inverse Fourier Transformation. The term enclosed in square brackets on the right-hand side of Eq. (8) is evaluated in the frequency domain and then transformed to the time domain as indicated.

Substituting Eq. (7) into the equation of motion of structure (1) enables the response of this structure–soil system to the incident seismic waves to be determined by a numerical integration scheme in the time domain. Details of the scheme used may be found in [1].

## 4. Modeling

### 4.1. Substructure method and direct method

The substructure method, which is employed in the scaled boundary finite-element method, can reduce the number of the degree of freedom by orders of magnitude when compared to the direct method. In a direct method, modeling of a significant part of soil is essential for accounting the radiation condition for an unbounded medium. The distance between the artificial soil boundary and the building is usually several times of the width of the structure. After a finite-element mesh, the soil will dominant the total number of nodes of the soil–structure system. Therefore, the direct method is usually used to study two-dimensional models. For a three-dimensional case, the direct method is far less efficient than substructure method. In the substructure method, a layer of the soil around the building’s foundation represents the soil. A force–displacement relationship is formulated by constructing a unit-impulse response matrix of the unbounded soil. The unbounded soil is rigorously modeled by using this analytical result. Consequently, the most number of degrees of freedom are generated in modeling the building structure, instead of the soil. Furthermore, the standard finite-element method is used to model the tall building because of its advantages of accuracy and convenient standard algorithms in the public domain.

### 4.2. Building model

In order to obtain a building’s deformation in an earthquake simulation, a symmetric building is simplified with uniform properties along its height. The tall building model is designed with 30 stories above the ground with a 5-story basement as shown in Fig. 2. Each story is  $18 \times 18 \times 3.5 \text{ m}^3$  and is divided into 8-node brick elements,  $4.5 \times 4.5 \times 3.5 \text{ m}^3$ . Then, each level has 16 brick elements. The number of the total elements for the 35-level building is 560. For civil engineering projects, this modeling has a small size of the number of degrees of freedom. Each node of the 8-node brick element has 3 degrees of freedom for translational movement in a rectangular Cartesian coordinate space. The interface element is a 4-node plate element with each node coincident with one of the structure’s element. The SSI interface can be divided into several parts for modeling the soil layers. In this paper, only one layer of soil is modeled. There are a total of 112 plate elements and 560

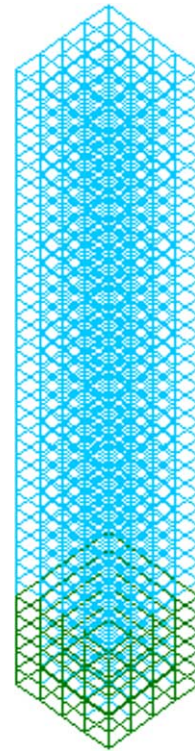


Fig. 2. Finite element model of a 30-story building with a 5-level basement. The green represents adjacent soil layer. The soil layer is modeled by using the scaled boundary finite elements which share the same plate element of the structure. The blue elements are the structural brick elements. (For interpretation of the references in colour in this figure legend, the reader is referred to the web version of this article.)

brick elements, and the total nodes are 900. The dynamic stiffness matrix has 2700 degrees of freedom.

#### 4.3. Cartesian coordinate system

The origin of the Cartesian coordinate system is assigned to be at the center of the first level, where the building's centerline intersects the ground surface. The Z-axis is pointing downward into the half space. The X–Y plane is the ground surface. The building is symmetric about the coordinate planes, X–Z and Y–Z. We select the X–Z plane as the input plane without losing the generalization. The input angle is measured from the positive X-axis to the direction of the wave propagation. In this study, a seismic recording is input at the origin of the coordinate system, which is the control point.

#### 4.4. Soil properties

Soil properties are assigned to the nodes on the interface with the building. The soil properties vary according to the different layers. In this study, the displacement of the buildings at the ground level is of most interest. The dynamic response of the buildings depends on the soil properties and damping ratios of the soil and buildings.

### 5. Numerical results

The first example investigates the response of a 30-story building, with a 5-level basement, subjected to P-, SH-, and SV-waves from 90°, 60°, and 30° measured from the horizontal direction. The displacements of each story are obtained and compared between different cases with different input angles for one input wave type or between different wave types. The building is assumed to stand on soft soil instead of fixed or semi-fixed on a rock bed. In this study, we use the consistent mass matrix without mass lumped damping as mentioned above.

In an actual experiment by using a test table to simulate the ground motion, the input motion is usually along two orthogonal horizontal directions and one vertical direction. The acceleration-time history data is the source of signals. In this numerical example, the scheme is to assign the input body wave with an angle measured from the horizontal direction to the propagation direction, which simulates real wave motion in the unbounded soil.

In order to obtain the response of various tall buildings subjected to identical seismic recordings, 5-, 10-, 20-, and 30-story buildings were modeled and simulated; each with 5-level basements. The 5-, 10-, 20-, and 30-story buildings are noted as models A, B, C, and D, respectively.

The amplitudes of the displacements along the height of the other three buildings are compared with the 30-story building, subjected to same input motion. The effects of the building's configurations on the influence of its vibration and deformation in the event of simulation are obtained. This can be used to explain the phenomenon that at the site impacted by severe ground motion, buildings of different heights experience different damage. Usually, the most damage occurs to middle size residential buildings because their fundamental frequencies are in the range of low frequency intervals of the earthquakes.

By using the dynamic analysis in the frequency domain, the natural frequency and corresponding vibration mode shape can be obtained. In this study, the dynamic linear elastic analysis is carried out for tall buildings in the time domain. Torsional movement is not considered in this study, and the bending of the building is expressed as an equivalent translational displacement. Through this numerical method, the overall deformations of tall buildings, subjected to severe ground motion, are obtained.

The peak displacements (PD) of the building during vibration are recorded and used to analyze the dynamic behaviors of the tall buildings subjected to earthquakes. The difference between PD and the displacement at any time interval is that the PD represents the largest deformation that occurred during that time interval. The displacements of the nodes are relative to the static position before the input of the seismic waves.

#### 5.1. Non-dimensional scheme

In this study, a non-dimensional scheme is used. The building height  $H$  and shear wave velocity in the soil are used as the characteristic length and velocity, respectively. The characteristic time is represented as

$$\bar{t} = \frac{H}{c_s}$$

Therefore,

$$\bar{t} = \frac{t}{\bar{t}}, \quad \bar{u} = \frac{u}{H}, \quad \bar{c}_p = \frac{c_p}{c_s}, \quad \bar{c}_s = 1,$$

$$\bar{E}_b = \frac{E_b}{E_s}, \quad \bar{E}_s = 1, \quad \bar{\rho}_b = \frac{\rho_b}{\rho_s}, \quad \bar{\rho}_s = 1$$

are non-dimensional time, displacement, and P-wave velocity, S-wave velocity, Young's modulus and densities of the building and soil, respectively. The storey height  $H$  equals 3.5 m. The shear wave velocity  $c_s$  equals 774 m/s and dilatational wave velocity  $c_p$  equals 1341 m/s. The density of the concrete building  $\rho_b$  equals 2500 kg/m<sup>3</sup>, and the density of the soil  $\rho_s$  equals 2000 kg/m<sup>3</sup>. Young's modulus of the concrete building  $E_b$  equals 30 GPa, and Young's modulus of the soil  $E_s$ . Henceforth, the superposed bar will be omitted.

5.2. Case study for 30-story building

5.2.1. P waves

When a dilatational P wave is input vertically (measured 90° from the horizontal), the largest deformation occurs in the vertical axis direction, as shown in Fig. 3. During a strong earthquake (Tabas, 1978) with accelerations as high as 919.025 cm<sup>2</sup>/s, the basement level endures the greatest displacement. The displacement dramatically changes at the surface. The dilatational wave transfers the energy through the stress generated in the building, after the foundation is stressed by the vertically input wave. Because the model is axially symmetric, the horizontal displacements in the X and Y directions are largely of same fashion. The horizontal displacement amplitude is such relatively small compared with the vertical axial deformation in this case. When the earthquake wave incident angles are 60° and 30° angles, there are more horizontal components of energy transferred to the super structure, as shown in Figs. 3–5. The X direction amplitude of the displacement of the node in the centerline of the building becomes the dominant vibration component. This type of large continuously horizontal vibrations may damage the structure. Therefore, the shear strength of the structure is a very important factor for resisting earthquakes. The PD along the X direction increases to the same order of magnitude as the vertical PD when input angle is 60°; and even larger at 30°, which is closer to the horizontal plane. Since the seismic input plane is the X–Z plane, the X direction is influenced more than the Y direction. The energy dissipated by the inter-story drift also increases. When the P wave impacts the building with a smaller input angle, a larger displacement and consequently more damage will be observed. Therefore, the characteristics of deformation and vibration of

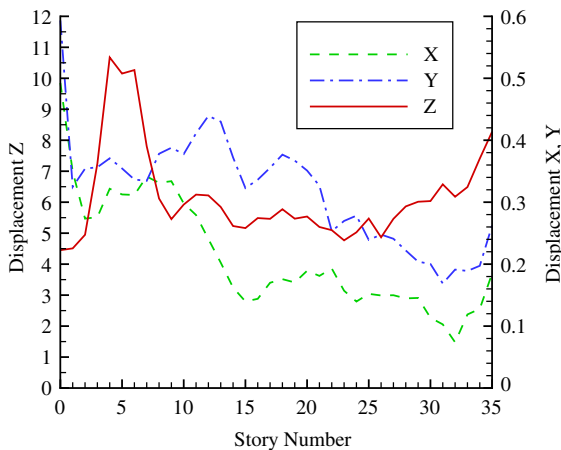


Fig. 3. Non-dimensional peak displacement of the centerline of the model D by vertically input P wave.

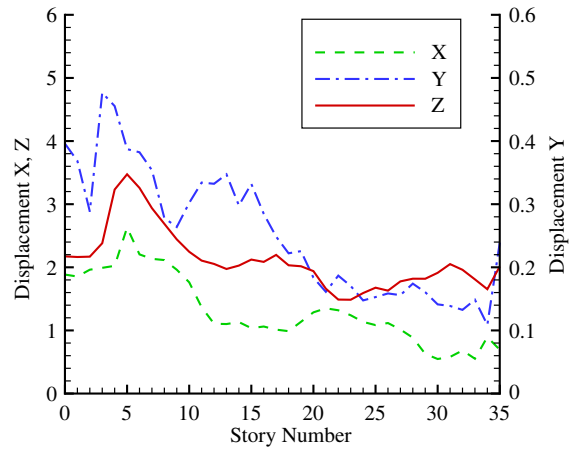


Fig. 4. Non-dimensional peak displacement of the centerline of model D by P wave at 60° input angle.

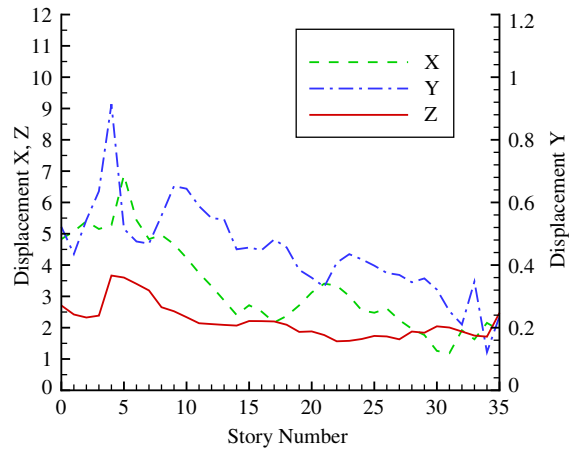


Fig. 5. Non-dimensional peak displacement of centerline of model D by P wave at 30° input angle.

buildings depend on the earthquake wave input angle for the case of dilatational waves.

5.2.2. Shear waves

The SH wave is a shear wave with the particle motion direction parallel to the ground surface, and vertical to the X–Z input plane. For an input angle of 60°, the main component of the deformation occurs in the Y direction. The building absorbs the kinetic energy with large deformations occurring at the ground level. As shown in Fig. 6, the PD is at a maximum at the ground level, decreases approximately proportional with the height of the building from the ground level to the roof. The X, Z displacements are much smaller components, which can be neglected.

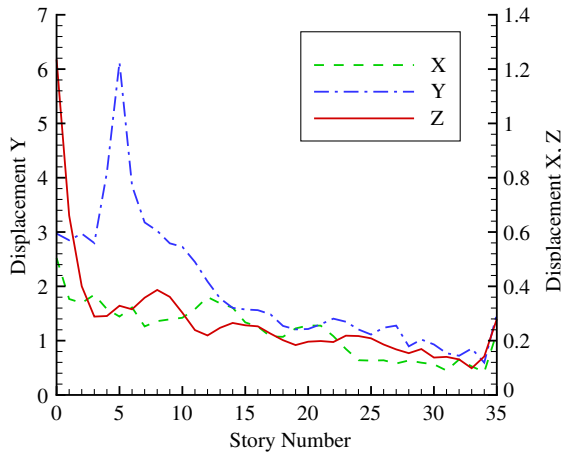


Fig. 6. Non-dimensional peak displacement of the centerline of model D by SH wave at 60° input angle.

The SV wave is a shear wave with the particle motion in a plane vertical to the ground surface and coincident with the *X–Z* input plane. In this case, the *X, Z* components are the main components of deformation for a wave input angle of 60°. As a result, most of the energy will be transferred in the input plane along the *X* and *Z* directions. As shown in Fig. 7, the maximum PD in *X* direction occurs at the level close to the ground and then rapidly decreases.

5.2.3. SSI effect

The relationship between the input wave type and the subsequent deformation of the buildings is influenced by the interaction between the soil and foundation. In this model, the unbounded soil is represented by the soil–

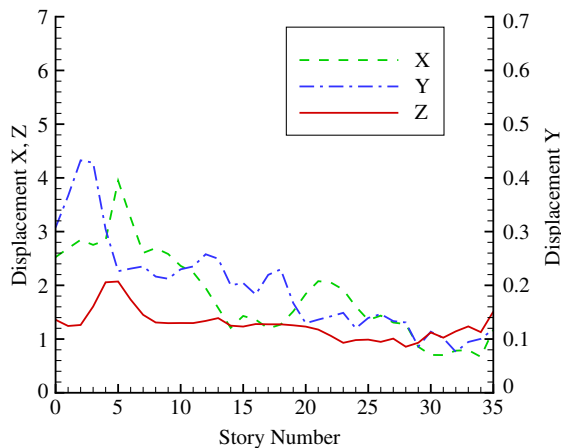


Fig. 7. Non-dimensional peak displacement of the centerline of model D by SV wave at 60° input angle.

structure interface and the ground motion is assigned control points, which simulates the motion due an earthquake. Thus large deformations of the foundation are expected. The more explicit SSI effects, such as separation occurring between the soil and foundation are not modeled here due to the complexity of this problem. This study shows that a rigid foundation has greater resistance to earth motion. Also, the large inter-story drift, between the ground floor and the middle floor, demands large shear strengths on the shear walls to resist an earthquake.

The SSI effect is demonstrated by the distribution of PD obtained in the analysis at the underground level. Because of the interaction between the structure and the adjacent soil, the motion of the soil influences the deformation of the building. Consequently, the peak values of deformation usually occur at the ground level, which is at the boundary between the soil and free surface.

5.3. Building factors

In order to compare the damage of buildings of different heights, and for different types of input ground motion, a group of four models A, B, C, and D are investigated.

For the P wave, at input angles of 60° and 90°, the buildings of shorter height have larger PD in the vertical direction, as shown in Figs. 8 and 9. The largest displacements occur for building heights in the range of 10–15 stories. By comparing the deformation in *X* direction, this illustrates that the buildings of shorter height have a greater horizontal drift from the original position than do taller buildings.

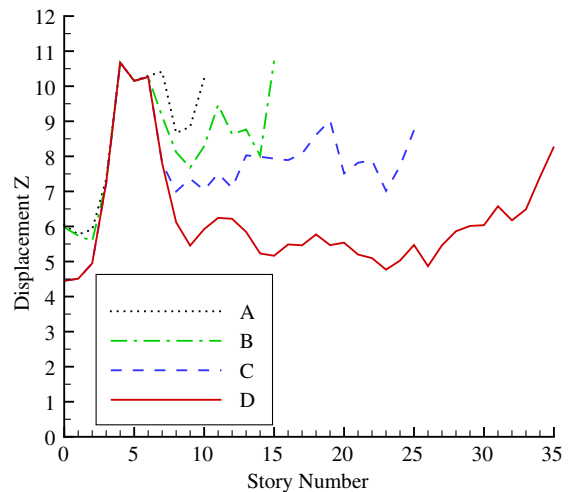


Fig. 8. Non-dimensional displacement of node in centerline of models by vertically input P wave.

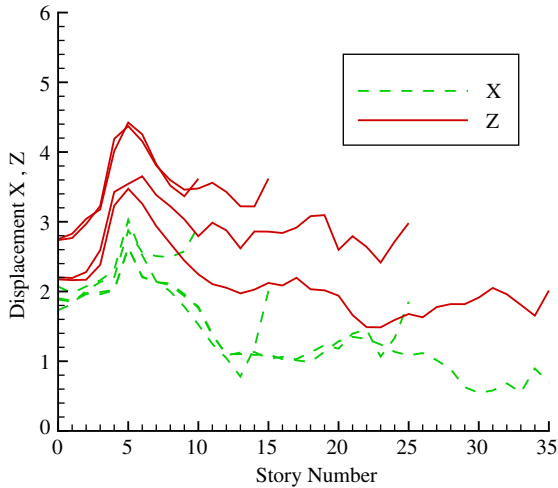


Fig. 9. Non-dimensional displacement of node in centerline of models by P wave at 60° input angle.

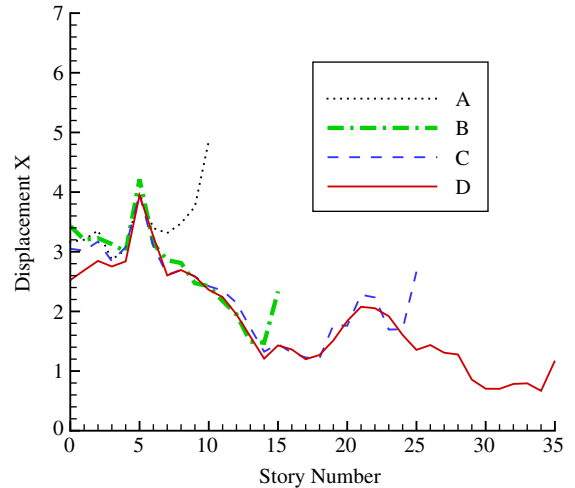


Fig. 11. Non-dimensional displacement of node in centerline of models by SV wave at 60° input angle.

As shown in Figs. 10 and 11, for both SH and SV waves, models B, C and D have similar slopes in the peak displacement along the horizontal directions, X or Y, when at the incident angle of 60°. The model A has the same slope when the input wave is a SH wave. It has a large drift that can be verified from the displacement-time history of the roof center. This study shows the response of buildings with different heights for one earthquake event. The taller building has less inter-story drift at upper levels; consequently the larger inter-story drift at lower heights may be the reason for causing structural failure during earthquakes of large magnitude. From field observations, the shorter residential

buildings, of 4–5 stories, are the most vulnerable to earthquakes of large magnitude.

5.4. Time history of the roof movement

The vertically input P wave case is interpreted in detail in this section. As shown in Fig. 12, models A and B start to move away from the static position after approximately 11 s and 16 s, respectively. The taller buildings C and D start to move from the static position around 25 s and 38 s, respectively. The negative value means the displacement is directed upwards, because the positive

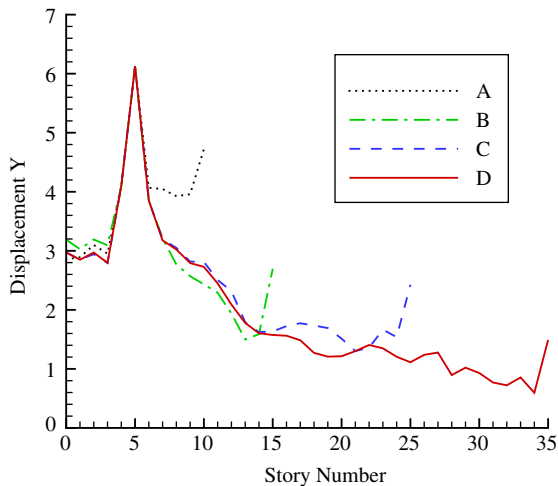


Fig. 10. Non-dimensional displacement of node in centerline of models by SH wave at 60° input angle.

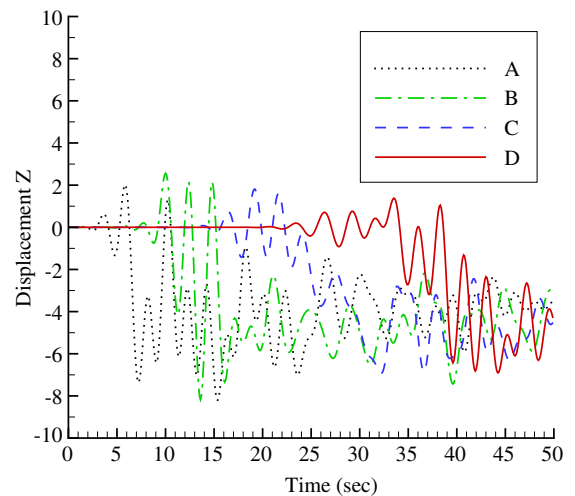


Fig. 12. Time history of the non-dimensional displacement for the roof center of the buildings for vertically input P wave.

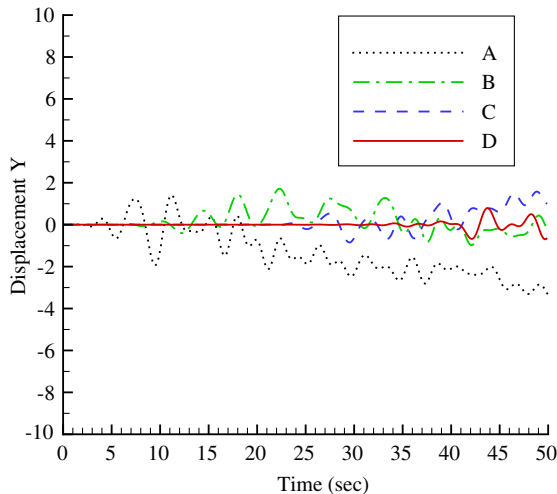


Fig. 13. Time history of the non-dimensional displacement for the roof center of the buildings for vertically input SH wave.

Z-axis is defined positive downwards into the soil half-space.

For SH waves, at an incident angle of  $90^\circ$ , the roof centers of models A and B, have greater displacements than models C and D. Again, from the time history shown in Fig. 13, the buildings' movement can be understood qualitatively. The Y component of the displacement of models A and B differ in directions after 18 s. For the same input wave, the direction preference for a symmetrical building depends on factors such as the building height, and natural frequency of the structure.

## 6. Conclusions

Based on a new numerical procedure for solving problems of wave–soil–structure interaction, we investigated the response of buildings, of four different heights, subjected to earthquakes of large magnitude. The peak displacement of the nodes on the axes of the buildings are obtained and compared by considering the SSI effects and building factors. The largest deformation of the buildings occurs at the basement levels, which are

close to the ground surface. P waves cause more deformation and movement along the input direction. Shear waves, SH and SV waves, cause much more inter-story drift which is vertical to the input direction. Also, the time histories of the displacement of the roofs show the dynamic vibration behavior of the buildings.

## References

- [1] Zhang X, Wegner JL, Haddow JB. Three dimensional soil–structure–wave interaction analysis in time domain. *Earthq Eng Struct Dynam* 1999;36:1501–24.
- [2] Wegner JL, Zhang X. Free vibration analysis of a three-dimensional soil–structure system. *Earthq Eng Struct Dynam* 2001;30:43–57.
- [3] Wolf JP. *Soil structure in the time domain*. Englewood Cliffs, NJ: Prentice-Hall; 1988.
- [4] Shah AH, Wong KC, Datta SK. Diffraction of plane SH waves in a half-space. *Earthq Eng Struct Dynam* 1982;10:519–28.
- [5] Mossessian TK, Dravinski M. Application of a hybrid method for scattering of P, SV, and Rayleigh waves by near-surface irregularities. *Bull Seismol Soc Am* 1987;77:1784–803.
- [6] Lysmer J, Kuhlemeyer RL. Finite dynamic model for infinite media. *J Eng Mech Div ASCE* 1969;95:859–77.
- [7] Smith WD. A nonreflecting plane boundary for wave propagation problems. *J Comput Phys* 1974;15:492–503.
- [8] Liao ZP, Wong HL. A transmitting boundary for the numerical simulation of elastic wave propagation problems. *J Comput Phys* 1984;3:174–83.
- [9] Wolf JP. *Dynamic soil–structure–interaction*. Englewood Cliffs, NJ: Prentice-Hall; 1985.
- [10] Song Ch, Wolf JP. The scaled boundary finite-element method–alias consistent infinitesimal finite-element cell method for elastodynamics. *Comput Methods Appl Mech Eng* 1997;147:329–55.
- [11] Wolf JP, Song Ch. *Finite-element modeling of unbounded media*. New York: Wiley; 1996.
- [12] Tehranizadeh M. Soil–structure interaction of tall building. In: *Proceedings of the 11th European Conference on Earthquake Engineering*, Paris. Rotterdam: Balkema; 1998.
- [13] Chen J. Analysis of local variations in free field seismic ground motion. Ph.D. Dissertation, University of California, Berkeley, 1980.